

OPEN

Carbon and Calcium Carbonate Export Driven by Appendicularian Faecal Pellets in the Humboldt Current System off Chile

A. Eduardo Menschel¹ & Humberto E. González^{2*}

The role of appendicularian faecal pellet (FPa) size fractions on coccolithophore-derived particulate organic carbon (POC) and calcium carbonate (CaCO₃) export to the deep sea was assessed from sediment traps within a period of ten years (1995–2004) off Coquimbo (CQ, 30°S) and five years (2005–2009) off Concepción (CC, 36°S) in the Humboldt Current System (HCS) off Chile. The composition and size distribution of 1,135 FPa samples from sediment traps deployed at 2,300 and 1,000 m depths showed non-linear, inverse relationships between the FPa size-fractions and their volume-specific POC and CaCO₃ contents, which were up to ten times higher for small (<100 μm in diameter) than large (>100 μm) FPa. On average, 13 and 2% of the total POC and CaCO₃ fluxes, respectively, were contributed mainly by small FPa (90%), with maxima during the autumn and summer. Thus, a non-linear, exponential model of volume-specific POC and CaCO₃ contents of FPa substantially improved vertical flux rate estimates. In the HCS, annual carbon flux based on a non-linear FPa carbon load was double the estimate assuming a linear-volume to carbon load for FPa (345 and 172 kton C y⁻¹). We recommend a widespread consideration of this non-linear model in global carbon estimates.

The Humboldt Current System (HCS) off Chile is one of the world's most productive coastal upwelling systems¹, originating from the West Wind Drift at circa 40–45°S² and including the Coquimbo (30°S) and Concepción (36°S) upwelling centres. The coastal and oceanic regions between 30°S and 36°S are dominated by Sub-Antarctic Waters (SAAW) down to 150 m depth and approximately 700 nm westward. This part of the HCS is highly dynamic with a net northward flow of the SAAW, which bifurcates into two tongues (oceanic and coastal currents) and border the southward Chile-Perú counter current^{3,4}. Below the SAAW down to 400 m depth lay the cold (<10 °C), nutrient rich, oxygen depleted (<1 mL L⁻¹)⁴ Equatorial Subsurface Water⁴. Between 400 and 1,000 m depths predominate the Antarctic Intermediate Waters and >1,000 the Deep Pacific Water. The region between 30–36°S is characterized as a transition zone with high kinetic energy (>40 cm² s⁻²) in a wide band parallel to the coast that can extend up to 800 km westward⁵.

The wind stress that favours upwelling along the coast off Chile predominates during spring-summer and contributes to fertilization (e.g. nitrate, phosphate) that promotes high primary production (>20 g C m⁻² d⁻¹) and phytoplankton biomass (>5 mg m⁻³) in the surface waters of the HCS⁶. The importance of the continental margins in the productivity and carbon cycles is widely recognized^{7–9}; however, the little information on the function of the biological pump is restricted to specific upwelling centres within the vast area covered by the HCS^{10–12}.

The biological carbon pump is an important component of the global carbon cycle in which the factors influencing zooplankton faecal material export, particularly PFa, remain poorly understood¹³. In the coastal areas of the HCS, the vertical flux of POC is driven mainly by diatoms and copepods⁶; however, in oceanic areas, the carbon flux is driven mainly by appendicularian/euphausiid faecal pellets and the carbonate flux by foraminifers and FPa loaded with coccolithophore shells. Thus, in oceanic areas of the HCS off Chile, appendicularians and coccolithophores are important functional groups in the carbonate pump^{6,14,15}. Overall, the magnitude and

¹Programa Doctorado en Oceanografía de la Universidad de Concepción and Instituto de Ciencias Marinas y Limnológicas, Universidad Austral de Chile, Research Centre on Dynamics of High Latitude Marine Ecosystems (FONDAP-IDEAL), Casilla, 567, Valdivia, Chile. ²Instituto de Ciencias Marinas y Limnológicas, Universidad Austral de Chile, Research Centre on Dynamics of High Latitude Marine Ecosystems (FONDAP-IDEAL), Casilla, 567, Valdivia, Chile. *email: hgonzale@uach.cl

Station	Position		Trap depth (m)	Bottom depth (m)	Samples	Deployment period		Interval (d)
						Start	End	
CQ	30°S	73°11'	2,300	4,700	20	28 Jan 1995	22 May 1995	7
	30°S	73°11'	2,300	4,700	9	18 June 1995	14 Sept 1995	7
	30°S	73°11'	2,300	4,700	20	28, Jan 1996	28 June 1996	9
	30°S	73°11'	2,300	4,700	20	14 Feb 1997	19 Oct 1997	14
	30°S	73°11'	2,300	4,700	18	15 Nov 1997	19 June 1998	13
	30°S	73°11'	2,300	4,700	20	11 Feb 1999	01 Aug 1999	10
	30°S	73°11'	2,300	4,700	6	14 Sept 2000	03 Dec 2000	17
	30°S	73°11'	2,300	4,700	15	15 Apr 2002	25 Nov 2002	17
	30°S	73°11'	2,300	4,700	12	05 Apr 2003	07 Oct 2003	18
	30°S	73°11'	2,300	4,700	5	22 May 2004	29 July 2004	18
CC	36°59'S	74°49'	1,000	4,400	16	12 Dec 2005	20 Sept 2006	19
	36°59'S	74°49'	2,300	4,400	20	18 Oct 2006	25 Sept 2007	19
	36°59'S	74°49'	2,300	4,400	20	27 March 2008	04 March 2009	19

Table 1. Station positions of the sediment traps off Coquimbo (CQ) and Concepción (CC) sites, trap depths, bottom depths at the trap locations, numbers of samples retrieved without problem, deployment periods and sampling intervals. Sample numbers less than 20 indicate periods when the sediment trap malfunctioned. The total samples obtained from sediment traps (CQ and CC) were 201. In the column “Samples”, the numbers <20 indicate malfunction of the sediment trap.

efficiency of the total POC flux temporally and spatially depend on changes in zooplankton and phytoplankton community compositions, as well as on changes in the biological processes (i.e. zooplankton grazing rate, faecal pellet production rate, phytoplankton aggregation, microbial degradation) that affect the dynamics of particle flux from the euphotic zone in oceanic provinces¹⁶ and upwelling areas off central Chile¹².

In the HCS, El Niño (EN) events show oceanographic changes such as intrusion of oceanic, low-nutrient, warm, oxygenated waters into the coastal areas that trigger positive sea-surface temperature anomalies. During EN events, the plankton assemblages shift to smaller species during the warm phase; however, the total phytoplankton biomass, primary production, and vertical flux of carbon do not change^{3,17–19}. Conversely, during “La Niña” events, the shallowed nutricline leads to increased nutrient supply, phytoplankton biomass, and primary production²⁰.

Several hundred sediment trap studies since the 1970s have reported the pivotal role of zooplankton faecal pellets (FP) in the carbon biogeochemical cycle^{14,21–23}. This plethora of information demonstrates the importance of zooplankton FP in the export of particulate organic carbon (POC) from the photic zone to the deep sea^{24,25}. The contributions of FP produced by different functional groups, including euphausiids, appendicularians, copepods, salps, and microzooplankton, to vertical flux of POC also have been reported^{24–26}, where appendicularians stand out because of their high FP production rates (Supplementary Table S1) and carbon fluxes (Supplementary Table S2), but relatively low sinking rates (Supplementary Table S3). The high variability of those estimates seems to relate to many physical and biological interactions that affect export versus recycling of the carbon and nitrogen in FP. For example, appendicularians usually represent a minor fraction of total mesozooplankton biomass; however they can process large amounts of food in a short time and produce numerous FP that contribute to export production^{27,28}, playing significant roles in the export of the POC¹⁴ and calcium carbonate (CaCO₃) to the deep sea^{6–29} in many disparate areas of the world’s oceans.

Coccolithophores also are an important component of the phytoplankton in the HCS off Chile and the world ocean^{6,30,31}. Their transport to deep layers of the ocean has been principally by means of FP, where a linear relationship between POC or CaCO₃ contents with volume-derived FP size has been assumed³². The reasoning is that the shells (coccoliths) increase the FP sinking speed³³, although there is little information on the appendicularian diets and the physical and chemical composition of FP, which are usually assumed to be invariable and independent of the size of the animal and the extruded faecal pellet. We tested this assumption in order to determine the role of FP of different sizes in the fluxes of POC and biogenic carbonate to the deep sea at two sites (CQ, 30°S; and CC, 36°S) (Table 1), in the HCS off Chile (Fig. 1).

Results

FPa size-spectrum. The size-spectrum of FPa sizes (diameter and length) and volumes were analysed from 5,102 FPa isolated from 201 sediment trap samples from CQ and CC in the HCS, covering most of the study period. We found that 89% of the FPa were between 10 and 100 µm in diameter, highlighting the pivotal role of small FPa in fluxes of carbon and calcium carbonate in the oceanic region of the HCS off central Chile (Fig. 2). The remaining FPa (11%) were between 101 and 390 µm.

Carbon and calcium carbonate contents in FPa. The inverse relationship between the FPa size fractions and their volume-specific POC content (mg C mm⁻³) was best represented by a power function ($f(x) = 0.0087x^{-0.556}$; $R^2 = 0.85$). This was obtained from measurements of 1,135 FPa isolated from sediment trap samples collected at stations CQ and CC during most of the study period. The POC in FPa was highly variable (0.02–0.77 mg C mm⁻³), with the highest volume-specific values (~0.2–0.77 mg C mm⁻³) in small FPa (Fig. 3a)

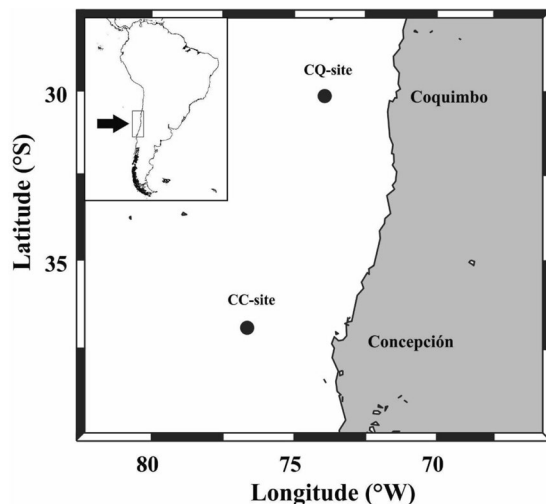


Figure 1. Locations of sediment traps deployed for determination of carbonate flux from appendicularian faecal pellets in the CQ (30°S) and CC (36°S) sites in the Humboldt Current System off Chile.

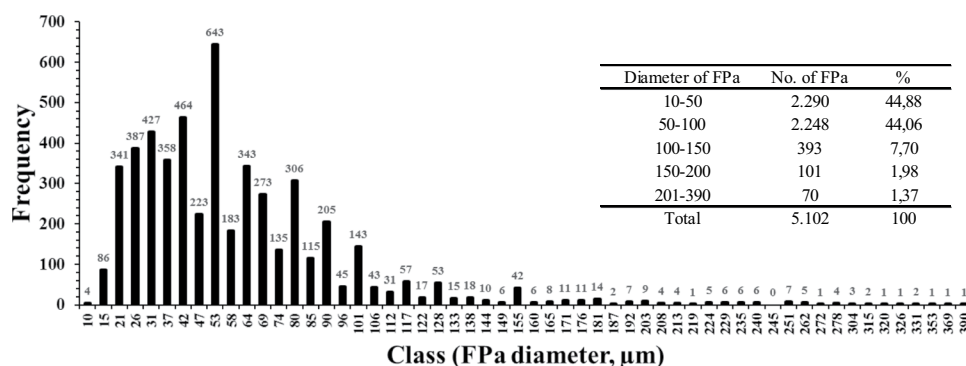


Figure 2. Frequency distribution of appendicularian faecal pellet (FPA) size fractions quantified from sediment trap samples deployed at the CC and CQ sites in the Humboldt Current System off Chile. The numbers of FPA per 5- μm size interval are shown above each bar. The numbers and percentages (%) of FPA in 50- μm size intervals are in the inset table. A total of 5,102 FPA were measured from 201 sediment trap samples (145 from the CQ and 56 from the CC sites).

and the lowest ($0.02\text{--}0.2\text{ mg C mm}^{-3}$) in large FPA (Fig. 3). We also expressed the average concentration of carbon per FPA (mg C FPa^{-1}) for each size group (small, medium, and large) as functions of their average biovolumes. Different slopes in each of the linear equations among the three size groups denote a highly non-linear and inverse relationships between FPA carbon content and their biovolumes in FPA (Fig. 3b–d).

Coccolith abundance, CaCO_3 content, and coccolithophore composition within FPA. The number of coccolithophore plates in the FPA matrix were quantified by species. The FPA ranged between $0.08\text{--}0.35\text{ mm}$ in diameter and $0.0006\text{--}0.080\text{ mm}^3$ in biovolume. The coccolith abundance and coccolithophore-derived calcium carbonate (CCa) concentration showed non-linear inverse exponential functions when related with its biovolume-specific (per mm^3) value at both sites. At CQ, the mean coccolith and CCa contents were 5.1 to 24.3×10^6 coccoliths mm^{-3} and 0.1 to $0.3\text{ mg CaCO}_3\text{ mm}^{-3}$, respectively. The maximum biovolume-specific abundance of coccoliths and CCa were observed in the smallest FPA (2.1×10^7 coccoliths mm^{-3} ; $0.24\text{ mg CaCO}_3\text{ mm}^{-3}$) and the minimum in the largest (1.3×10^7 coccolith mm^{-3} ; $0.18\text{ mg CaCO}_3\text{ mm}^{-3}$) (Fig. 4a,b). In contrast, at the CC site, these parameters ranged from 7.8×10^6 coccoliths mm^{-3} and $0.091\text{ mg CaCO}_3\text{ mm}^{-3}$ to $2.9 \times 10^6\text{ mm}^{-3}$ and $0.027\text{ mg CaCO}_3\text{ mm}^{-3}$, respectively. The smallest FPA showed higher coccolith abundance and CCa concentration (6.2×10^6 coccoliths mm^{-3} ; $0.064\text{ mg CaCO}_3\text{ mm}^{-3}$); in contrast, the largest FPA had the least (5.5×10^6 coccoliths mm^{-3} ; $0.056\text{ mg CaCO}_3\text{ mm}^{-3}$) (Fig. 4a,b).

On average, seventeen genera/species of coccolithophore were found in the FPA from both sites; however, there were important differences between the CQ and CC sites. The abundance of coccoliths and CCa concentrations were ~ 3 and 1.6 times higher in CQ than in CC site. The main coccolith type observed was *Emiliania huxleyi*, which represented $>70\%$ of the abundance of all recorded species and was ~ 3 times more abundant in CQ than the CC site.

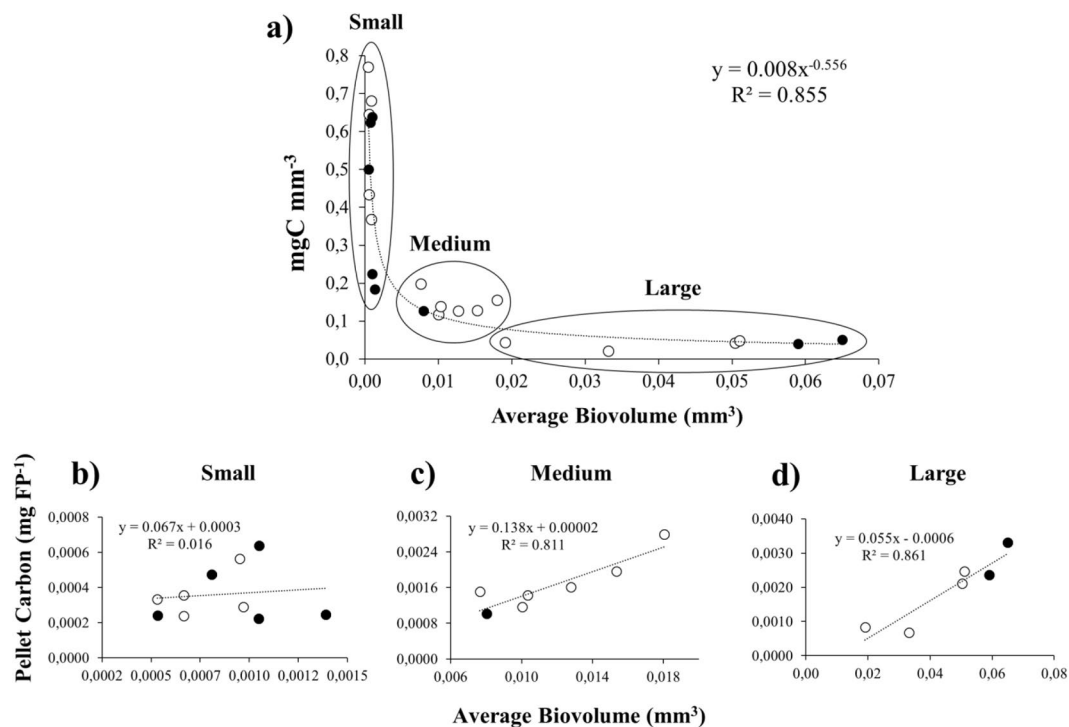


Figure 3. (a) Relationship between volume-specific carbon content (mg C mm^{-3}) and average biovolume (mm^3) for appendicularian faecal pellets (FPA) from the CQ (empty circles) and CC (filled circles) sites off Chile. (b–d) carbon contents of three different FPA size groups in relation to average biovolume: (b) small, (c) medium, and (d) large.

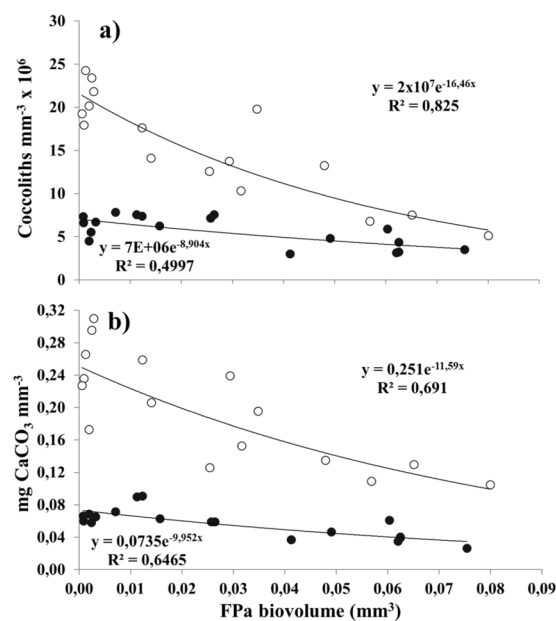


Figure 4. (a) Coccolith concentration (average number of coccoliths per $\text{mm}^3 \times 10^6$) and (b) CaCO_3 concentration in FPA ($\text{mg CaCO}_3 \text{mm}^{-3}$) as a function of appendicularian faecal pellets (FPA) biovolume (mm^3) in samples from the CQ (empty circle) and CC (filled circle) sites off Chile.

The CCa concentrations in FPA were dominated by coccoliths belonging to the species *Calcidiscus leptoporus*, which contributed ~45% of total carbonate biomass, while *E. huxleyi* and *Helicosphaera carteri* together contributed ~40%. These three species represented >80% of the carbonate biomass in FPA in both sites (Table 2).

Concepción (CC site)				Coquimbo (CQ site)								
Main	Coccoliths per FPa	SD Coccoliths per FPa	CaCO ₃ (pg) per coccolith (*)	CaCO ₃	SD CaCO ₃	CaCO ₃	Coccoliths per FPa	SD Coccoliths per FPa	CaCO ₃ (pg) per coccolith (*)	CaCO ₃	SD CaCO ₃	CaCO ₃
coccolithophore species	mm ³	mm ³		(mg μm ⁻³)	(mg μm ⁻³)	(%)	mm ³	mm ³		(mg μm ⁻³)	(mg μm ⁻³)	(%)
<i>Calcidiscus leptoporus</i>	388,977	142,845	79.5	1.8×10^{-12}	2.2×10^{-12}	46.955	1,144,288	412,790	79.5	2.7E-12	2.3×10^{-12}	44.345
<i>Emiliania huxleyi</i>	4,610,351	1,535,543	2.36	7.8×10^{-13}	9.6×10^{-13}	20.728	11,942,614	5,212,936	2.36	1.1E-12	7.8×10^{-13}	17.230
<i>Helicosphaera carteri</i>	80,238	33,545	138.9	7.1×10^{-13}	1.2×10^{-12}	18.876	254,033	147,097	138.9	1.2E-12	1.4×10^{-12}	20.166
<i>Gephyrocapsa mullerae</i>	282,634	156,164	8.00	1.5×10^{-13}	2.2×10^{-13}	3.980	1,189,431	764,395	8.00	3.4E-13	4.6×10^{-13}	5.512
<i>Gephyrocapsa oceanica</i>	56,616	44,208	20.2	8.0×10^{-14}	1.7×10^{-13}	2.110	389,992	350,497	20.2	1.6E-13	9.7×10^{-14}	2.639
<i>Syracosphaera pulchra</i>	60,720	36,223	14.75	7.0×10^{-14}	9.7×10^{-14}	1.856	57,357	44,161	14.75	2.1E-14	1.8×10^{-14}	0.337
<i>Helicosphaera spp.</i>	5,084	4,751	138.9	5.5×10^{-14}	1.0×10^{-13}	1.445	44,502	38,867	138.9	1.6E-13	1.3×10^{-13}	2.568
<i>Radobosphaera clavigera</i>	7,335	4,492	67.5	4.7×10^{-14}	8.0×10^{-14}	1.252	23,863	28,640	67.5	3.2E-14	3.1×10^{-14}	0.527
<i>Scyphosphaera apsteinii</i>	996	2,071	540	3.7×10^{-14}	1.0×10^{-13}	0.979	6,577	8,000	540	1.4E-13	1.9×10^{-13}	2.280
<i>Umbilicosphaera sibogae</i>	25,610	13,103	17.3	3.5×10^{-14}	5.7×10^{-14}	0.928	363,557	223,348	17.3	2.2E-13	2.6×10^{-13}	3.570
<i>Coccolithus pelagicus</i>	1,332	1,207	130	1.9×10^{-14}	3.3×10^{-14}	0.491	463	679	130	3.6E-15	6.3×10^{-15}	0.058
<i>Pontosphaera syracusana</i>	1,617	1,693	65.9	1.0×10^{-14}	1.5×10^{-14}	0.267	4,057	6,379	65.9	7.9E-15	7.2×10^{-15}	0.128
<i>Florisphaera profunda</i>	9,862	42,986	0.17	6.2×10^{-16}	2.7×10^{-15}	0.016	764,319	362,900	0.17	3.9E-14	3.5×10^{-14}	0.635
<i>Gephyrocapsa mullerae (coccosphere)</i>	770	1,865	160	4.2×10^{-15}	1.2×10^{-14}	0.111	0	0	160	0	0	0.000
<i>Calcosolenia murrayi / brasiliensis</i>	6,718	8,216	0.1	4.4×10^{-17}	5.6×10^{-17}	0.001	31,701	34,090	0.1	1.1E-16	1.4×10^{-16}	0.002
<i>Gaaderia corolla</i>	1,665	2,255	0.1	1.3×10^{-17}	2.1×10^{-17}	0.000	0	0	0.1	0	0	0.000
<i>Syracosphaera anthos</i>	8,311	5,583	0.1	6.2×10^{-17}	8.4×10^{-17}	0.002	22,640	20,210	0.1	9.4E-17	1.3×10^{-16}	0.002
<i>Syracosphaera spp.</i>	24,690	26,425	0.1	1.1×10^{-16}	1.2×10^{-16}	0.003	33,490	48,167	0.1	1.3E-16	2.9×10^{-16}	0.002

Table 2. Coccolithophore species found in the matrix of appendicularian faecal pellets (FPa) collected in sediment traps deployed at the CC and CQ sites off Chile and their contributions to total average carbonate and standard deviation (SD). The species-specific abundance of coccoliths per mm³ of FPa was counted in 35 bunches of measured (volume calculated) and sonicated FPa (16 from CQ and 18 from CC). The species-specific CaCO₃ contents per coccolith (*) were taken from the literature⁶⁸. The total coccolith abundance was depicted in Fig. 4.

POC, PIC/POC ratios and CaCO₃ fluxes mediated by FPa in CQ and CC. Fluxes of POC and CaCO₃ in FPa at 2,300 and 1,000–2,300 m depths in the oceanic region off CQ and CC varied greatly during time series stations measured (with gaps due to malfunctions of the traps) in time periods of ten and five years (1995–2004 and 2005–2009), respectively (Figs. 5 and 6). Overall in the CQ site, the FPa-mediated fluxes averaged 18.1% of the total POC flux (average $4.7 \text{ mg m}^{-2} \text{ d}^{-1}$) (Fig. 5a,b) and 3.4% of the total FPa-mediated CaCO₃ flux ($48.1 \text{ mg m}^{-2} \text{ d}^{-1}$) (Fig. 5c,d).

In the CC site, FPa-mediated fluxes averaged 19.8% (3.1×100)/15.6 and 4% (0.86×100)/21.36 of the total POC flux to the 1,000 m (average $15.6 \text{ mg C m}^{-2} \text{ d}^{-1}$) and 2,300 m (average $21.4 \text{ mg C m}^{-2} \text{ d}^{-1}$), respectively. While that the general average was 7.7% of the total POC flux ($19.7 \text{ mg C m}^{-2} \text{ d}^{-1}$) (Fig. 6a,b and Table 3).

The total FPa-mediated CaCO₃ flux represented in average the 1.6% (0.81×100)/51.6 and 0.7% (0.32×100)/44.54 to the 1,000 m (average $51.6 \text{ mg CaCO}_3 \text{ m}^{-2} \text{ d}^{-1}$) and 2,300 m (average $44.5 \text{ mg CaCO}_3 \text{ m}^{-2} \text{ d}^{-1}$), respectively. However, considering both depth (1,000 and 2,300 m) the average was ~1% of the total FPa-mediated CaCO₃ flux ($46.7 \text{ mg CaCO}_3 \text{ m}^{-2} \text{ d}^{-1}$) (Fig. 6c,d).

The total PIC/POC ratios for the CQ site (1.2) was higher than for CC site (0.28). On the other hand, the PIC/POC ratio was slightly higher in the FPa from CC-site (0.037, from both depths), than for CQ-site (0.022), respectively (Table 3).

In the CQ site, maximum fluxes of FPa-mediated POC ranged between 2.3 and $4.4 \text{ mg C m}^{-2} \text{ d}^{-1}$ and occurred during summer-autumn 1995 (Fig. 5b), while in the CC site, the maximum values ($3.0\text{--}7.4 \text{ mg C m}^{-2} \text{ d}^{-1}$) occurred during the summer-autumn 2005–2006 and winter of 2006 (Fig. 6b). Similarly, fluxes of FPa-derived CaCO₃ for the CQ site were highest in summer-autumn of 1995, 1998, and 2002 ($6.0\text{--}9.8 \text{ mg CaCO}_3 \text{ m}^{-2} \text{ d}^{-1}$) (Fig. 5d), while high fluxes for the CC site ($1.5\text{--}1.6 \text{ mg CaCO}_3 \text{ m}^{-2} \text{ d}^{-1}$) occurred during the summer-autumn of 2005–2006 (Fig. 6d).

The average annual FPa-mediated POC fluxes in the CQ site were highest during 1995 ($1.78 \text{ mg C m}^{-2} \text{ d}^{-1}$) and 1999 ($1.04 \text{ mg C m}^{-2} \text{ d}^{-1}$) and lowest ($0.22 \text{ mg C m}^{-2} \text{ d}^{-1}$) during 2003 (Fig. 5d). For the CC site, the highest fluxes were recorded during 2005 ($6.9 \text{ mg C m}^{-2} \text{ d}^{-1}$) and 2006 ($2.4 \text{ mg C m}^{-2} \text{ d}^{-1}$) (Fig. 6b). Likewise, the average annual FPa-mediated CaCO₃ fluxes were highest during 1995 for the CQ site ($3.5 \text{ mg CaCO}_3 \text{ m}^{-2} \text{ d}^{-1}$) and 2005 for the CC site ($1.5 \text{ mg CaCO}_3 \text{ m}^{-2} \text{ d}^{-1}$); and lowest during 2004 ($0.32 \text{ mg m}^{-2} \text{ d}^{-1}$) and 2008 ($0.1 \text{ mg m}^{-2} \text{ d}^{-1}$).

For the CQ site, the FPa-mediated POC flux during 1995 ($1.78 \text{ mg C m}^{-2} \text{ d}^{-1}$) was statistically different (Mann-Whitney test, $n = 16$, $p < 0.01$) from all other years combined; similarly, 1996–1998 ($0.6\text{--}0.8 \text{ mg C m}^{-2} \text{ d}^{-1}$) was statistically different from 2002–2003 ($0.3\text{--}0.2 \text{ mg C m}^{-2} \text{ d}^{-1}$) (Mann-Whitney test, $n = 13$, $p < 0.05$).

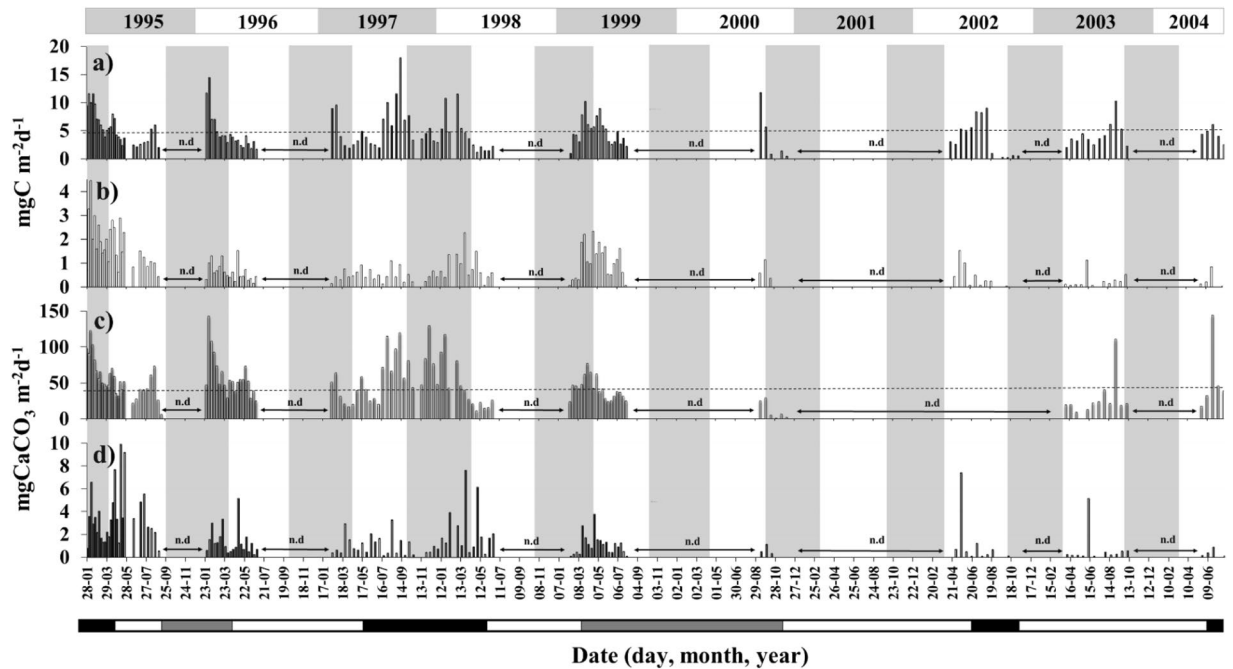


Figure 5. (a) Total particulate organic carbon (POC) flux ($\text{mg C m}^{-2} \text{d}^{-1}$) within the period 1995–2004 off Coquimbo (30°S) at 2,300 m depth. (b) Appendicularian faecal pellet (FPA)-mediated POC flux derived from a FPA non-linear, volume-specific POC model. (c) Total carbonate flux and (d) FPA-mediated carbonate flux ($\text{mg CaCO}_3 \text{ m}^{-2} \text{d}^{-1}$). The dashed line in (a) represents the mean total POC flux ($4.7 \text{ mg C m}^{-2} \text{d}^{-1}$) and the dashed line in (c) represents the mean total carbonate flux ($48.1 \text{ mg CaCO}_3 \text{ m}^{-2} \text{d}^{-1}$). The top bar represents the period between 1995 and 2004 while the vertical shading in gray represents the spring-summer periods. The bar at the bottom shows “El Niño” (black), “La Niña” (gray), and “normal” (white) periods (www.cpc.noaa.gov/products/analysis_monitoring/ensostuff/ensoyears.shtml). n.d. along the horizontal axes show periods of no data due to equipment failure.

High seasonal variability in FPA-mediated fluxes of POC and CaCO_3 was observed, with maxima in summer/autumn (1.2 and $2.1 \text{ mg m}^{-2} \text{d}^{-1}$) and minimum values in spring (0.4 and $0.6 \text{ mg m}^{-2} \text{d}^{-1}$, respectively). Fluxes differed statistically (Mann-Whitney test, $n = 31$, $p < 0.05$) between summer and winter-spring and between autumn and winter-spring.

For the CC site, fluxes of FPA differed significantly (Mann-Whitney test, $N = 18$, $p < 0.05$) among all years, except when we compared the pairs 2006–2009 and 2007–2009 that were similar (Fig. 6b,d). No significant seasonal differences in FPA-mediated POC or CaCO_3 were observed (Mann-Whitney test, $N = 35$, $p > 0.05$) during El Niño, La Niña, or “normal” periods (see Figs 5 and 6) in either of the two study areas (Mann-Whitney test, $N = 11$, $p > 0.05$).

Discussion

The Biological Carbon Pump is an important component of the global carbon cycle in which the factors influencing zooplankton faecal material export efficiency and its controlling factors, particularly for PFA export, remain poorly understood. Overall, the magnitude and efficiency of the total POC flux in time and space depend on changes in the zooplankton and phytoplankton community compositions, as well as on changes in biological processes (i.e. zooplankton grazing rate, FP production rate, phytoplankton aggregation, microbial degradation) that affect the dynamics of particle flux from the euphotic zone in oceanic provinces¹⁶ and upwelling areas off central Chile¹¹. The bulk of the faecal material usually is removed quickly from the upper water column due to microbial degradation and zooplankton activity^{34,35}, although zooplankton faecal material still is a prominent fraction of total POC export in many areas of the world oceans^{13,14}.

The composition of the faecal material collected in sediment traps deployed at the CQ and CC sites was represented mainly by three functional groups: appendicularians, euphausiids, and undetermined (where high degradation, amorphous or broken pieces precluded classification).

Published estimates of the POC content of FPA and its contribution to carbon export from the HCS have assumed an average carbon:volume ratio of $0.048 \text{ mg C mm}^{-3}$ ^{14,32}, but we demonstrated in this study that FPA size and both carbon and carbonate contents were related non-linearly (Figs 3a, 4b). For example, the mean carbon content per mm^{-3} in small FPA was five times higher than in large FPA (0.26 and 0.041 C mm^{-3} , respectively). This result is important for quantitative estimates of the biological pump intensity, assuming that the PFA contents would be released in the same proportions as found in the sediment traps in this study, where more than 90% of the FPA were small. Our exponential conversion increased the contribution of the FPA-mediated carbon flux by ~50% ($1.04 \text{ mg C m}^{-2} \text{d}^{-1}$) over that obtained using a linear conversion factor between carbon content and FPA-size¹⁴.

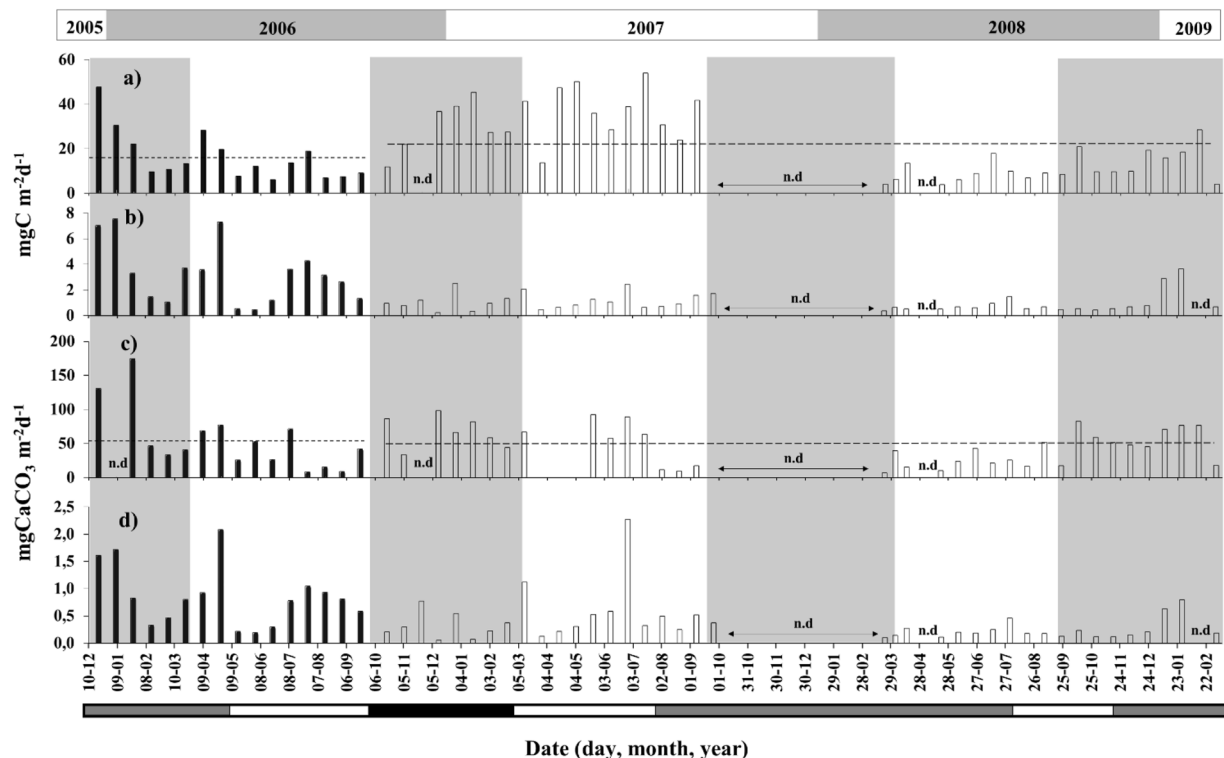


Figure 6. (a) Total particulate organic carbon (POC) flux estimated in sediment traps deployed in CC at 1,000 m depth (20/Dec/2005 to 20/Sept/2006, black bars) and 2,300 m depth (22/Sept/2006 to 04/Mar/2009, empty bars); (b) appendicularian faecal pellet (FPA)-mediated POC flux ($\text{mg C m}^{-2} \text{d}^{-1}$); (c) Total carbonate flux and (d) FPA-mediated carbonate flux ($\text{mg CaCO}_3 \text{ m}^{-2} \text{d}^{-1}$). The top bar represents the period between 2005 and 2009 while the vertical shading in gray represents the spring-summer periods. The bar at the bottom shows “El Niño” (black), “La Niña” (gray), and “normal” (white) periods. The dashed line upper of the black bar in (a) represents the mean total POC flux ($15.6 \text{ mg C m}^{-2} \text{d}^{-1}$) to 1,000 m of depth, while the dashed line upper of the empty bar show the average of the 2,300 m of the depth. The dashed line in (c) represents the mean total carbonate flux ($51.6 \text{ mg CaCO}_3 \text{ m}^{-2} \text{d}^{-1}$) to the 1000 m of depth, while that the dashed line upper the empty bar showed the mean $44.5 \text{ mg CaCO}_3 \text{ m}^{-2} \text{d}^{-1}$ of the 2,300 m of depth. n.d. along the horizontal axes show periods of no data due to equipment failure.

The calcareous components found in the matrix of FPa from the CQ and CC sites were mainly coccolith plates (mean 10.3×10^6 plates mm^{-3} , Fig. 4A), from which the most abundant coccoliths were *Calcidiscus leptoporus*, *Helicosphaera carteri* and *Emiliania huxleyi*, which together averaged 86% of the CCa or $2.4 \times 10^{-13} \text{ mg CaCO}_3 \mu\text{m}^{-3}$ in FPa isolated from sediment trap samples deployed at the CQ and CC sites (Table 2).

While existence of coccoliths and coccospheres embedded in the matrix of FPa have been reported²⁸, but no prior quantitative information on their contribution to carbonate flux in the ocean has been previously made. The coccoliths and coccospheres within the matrices of FPa are important in the export of carbonate and increase the sinking velocity of FPa to the deep ocean. Previous work has demonstrated that 1-mm particles that are 90% carbonate by mass (and 10% POM) sink ~fivefold faster than particles that are 60% carbonate by mass (and 40% POM) and ~1.75 times faster than particles that are 90% silicate by mass (and 10% POM)³³. An individual coccolith has a sinking velocity of 0.1 m d^{-1} or slightly higher, depending on species types and calcification degree. For example, *E. huxleyi*, *G. oceanica*, and *C. leptoporus* coccolith settling velocities (0.3 , 0.7 , and 4.3 m d^{-1} , respectively) were higher than diatom sinking rates, which ranged from 0.07 m d^{-1} (*Thalassiosira weissflogii*) to 0.2 m d^{-1} (*Thalassiosira oceanica*)³⁶. This information clearly suggests that FPa loaded with coccoliths and coccospheres can reach a higher sedimentation velocity than one loaded with diatom frustules, demonstrating the effectiveness of coccoliths and coccospheres in the transport of carbon and carbonate to the deep ocean.

The absence of a linear relationship between FPa-size and POC and CaCO_3 content may be attributable to differences in the size spectrum of the food ingested, with small FPa being more uniform and compact than large FPa. To test this hypothesis, we isolated large and small FPa from a sediment trap deployed at 2,300-m depth during different seasons between 1995 and 2004 and analysed the particle content qualitatively. Large FPa contained many relatively large pieces of diatom frustules ($20\text{--}63 \mu\text{m}$ diameter), mostly from the genus *Pseudo-nitzschia*, but also from the abundant *Thalassiosira* spp. and *Planctoniella sol.* In addition, the remains of radiolarians (groups Spummellaria, Nasselaria, and Phaeodaria), tintinnid loricae (genera *Codonellopsis*, *Dictiocysta*, *Protorhabdonella*, *Undella*, and *Dadayiella*), and silicoflagellates, such as *Dictiocha fibula*, were frequently observed. In contrast, microscopic analysis of small FPa demonstrated a preponderance of coccoliths, with occasional remains of diatoms and tintinnid loricae embedded in the FPa matrix. Large oikopleurid species have food-concentrating filters

Study area	Depth sediment trap (m)	POC flux mg m ⁻² d ⁻¹	CaCO ₃ flux mg m ⁻² d ⁻¹	C-CaCO ₃ mg m ⁻² d ⁻¹	PIC/POC ratios	Reference
Panama Bight (5°22'N, 85°35'W)	2,590	11.20	184.20	22.10	1.97	Honjo (1982) ⁴⁵
Station P (501 N; 1451 W)	3,800	10.50	67.90	8.15	0.78	Honjo (1984) ⁴⁶
Arabian sea (14.51 N; 651 W)	2,800	1.20	11.82	1.42	1.18	Nair <i>et al.</i> ⁴⁷
Equatorial Pacific (121 S; 135°W)	3,600	0.70	16.00	1.92	2.74	Honjo <i>et al.</i> ⁴⁸
Bay of Bengal (131 N; 841E)	2,300	6.70	42.13	5.06	0.75	Ittekkot <i>et al.</i> ⁴⁹
Humboldt current (30°S 73°11'W)	3,700	7.50	94.70	11.36	1.61	Hebbeln <i>et al.</i> ³
Humboldt current (30°S 73°11'W)	2,300	7.50	82.39	9.89	1.69	Hebbeln <i>et al.</i> ³
Subantarctic zone (53°02'S; 174°44'W)	1981	2.70	18.60	2.23	0.83	Honjo <i>et al.</i> ⁵⁰
Subantarctic zone (60°17'S; 170°03'W)	1,003	6.30	35.10	4.21	0.67	Honjo <i>et al.</i> ⁵⁰
West Sargasso Sea (31°50'N; 64°10'W)	3,200	2.40	22.40	2.69	1.12	Conte <i>et al.</i> ⁵¹
West Sargasso Sea (31°50'N; 64°10'W)	1,500	1.70	21.00	2.52	1.48	Conte <i>et al.</i> ⁵¹
East China Sea slope (25°11'N; 122°58'E)	1,340–1,588	128.60	214.20	25.70	0.20	Hung <i>et al.</i> ⁵²
Humboldt current (30°S 73°11'W)	2,300	7.00	61.00	7.32	1.05	González <i>et al.</i> ¹⁴
Arabian Sea (16°18'N 60°30'E)	1,200	14.80	106.80	12.82	0.87	Ramaswamy <i>et al.</i> ⁵³
Bay of Bengal (13°09'N 84°20'E)	2,282	8.50	39.50	4.74	0.56	Ramaswamy <i>et al.</i> ⁵³
Arabian Sea (03°34'N 77°46'E)	2,394	4.40	49.80	5.98	1.36	Ramaswamy <i>et al.</i> ⁵³
Bay of Bengal (05°01'N 87°09'E)	3,010	5.70	37.80	4.54	0.80	Ramaswamy <i>et al.</i> ⁵³
Humboldt current (30°S 73°11'W)	2,300	4.74 (0.86*)	48.12 (1.64*)	5.77 (0.19*)	1.22 (0.22*)	This Study
Humboldt current (37°05'S 74°50'W)	1,000	15.60 (3.10*)	51.62 (0.81*)	6.19 (0.097*)	0.39 (0.031*)	This Study
Humboldt current (37°05'S 74°50'W)	2,300	21.36 (0.86*)	44.54 (0.32*)	5.34 (0.038*)	0.25 (0.044*)	This Study
Humboldt current (37°05'S 74°50'W)	1,000/2,300	19.65 (1.51*)	46.66 (0.47*)	5.60 (0.056*)	0.28 (0.037*)	This Study

Table 3. POC, CaCO₃, C-CaCO₃ (mgC m⁻²d⁻¹) and PIC/POC ratios estimated from deep sediment traps (range 1,000–3,700 m depth) deployment in different areas of the world oceans. C-CaCO₃ correspond to inorganic carbon obtained from CaCO₃ bulk. (*) contribution of the FPa to the carbon and carbonate flux in the CQ and CC site in the HCS.

with a coarser mesh than small ones³⁷, suggesting a direct relationship between pore dimensions of appendicularian filters and body size. Our study suggested that large appendicularians utilized a broad food-size spectrum (diatoms, coccolithophores, tintinnids, radiolarians, etc.), while the diet of small appendicularians was more restricted, which partially explained the small mineral skeletons in small FPAs.

The FPa biovolume to POC (or CaCO₃) content models that should be used to estimate the role of FPAs in biomineral vertical fluxes follow size-dependent non-linear relationships, indicating that the FPa size fraction needs to be considered to improve the accuracy of these estimates. We strongly recommend a more taxa-specific analysis by microscopy, which is more time consuming but essential when dealing with size-dependent FPa-mediated POC and carbonate export processes. This view is supported by findings of changing composition of sinking particles across a region with unchanging carbon flux, suggesting that variability in the mechanisms of carbon flux³⁸ or the role of phytoplankton biominerals as ballast³⁹ may not be reflected by bulk measurements. In addition, coccolithophore calcium carbonate is usually considered to have a low carbon flux and high export efficiency²⁴. Thus, CCa is generally not included in calculations of FPa carbon export, resulting in up to 4% underestimation of total carbon flux to deeper areas of the HCS.

High seasonal and inter-annual variability in POC flux was observed in the time series station off the CQ site (Fig. 5). The estimated average FPa-driven POC flux at the CQ site (0.86 mgC m⁻² d⁻¹) was slightly higher than that reported for the same area during 1993–1995 (~0.7 mgC m⁻² d⁻¹)¹⁴, while that recorded for the CC site was substantially higher (1.5 mgC m⁻² d⁻¹) than at the CQ site (Figs 5b, 6b).

Overall, the use of the FPa-size-based carbon content model of this study increased the estimated contribution of FPAs to total POC export by a factor of 34% (CC site) and 46% (CQ site) over those obtained from a linear FPa-volume to carbon content model.

The highest average FPa flux occurred during the productive summer period, coinciding with intensification of the winds favouring upwelling and Ekman transport¹⁴, which may enhance local productivity and carbon export. We did not find significant differences ($p > 0.05$) in the FPa-mediated fluxes of POC or CaCO₃ among El Niño, La Niña, and “normal” periods (shown in Figs 5 and 6), suggesting that the diet of the appendicularians was not severely affected by these events.

Reports during the El Niño event in the HCS show that the seasonal upwelling ceases, the water column became warmer, and the thermocline and nutricline deepens significantly during the passage of coastal-trapped waves^{40,41}. These events decrease phytoplankton productivity and alter the trophic chain, changing the biological composition and physical dynamics of the coastal and marine ecosystems^{18,41}. Both phytoplankton and zooplankton shift toward small-sized species that have been claimed to prevail during El Niño^{17,18,40}. Thus, it is highly probable that the composition and size spectrum of small food particles used by appendicularians, down to colloids (<0.2 μm)⁴², is little affected by El Niño events^{37,43}, a situation that might be extrapolated to future global warming scenarios on the FPa-mediated carbon and CaCO₃ export fluxes.

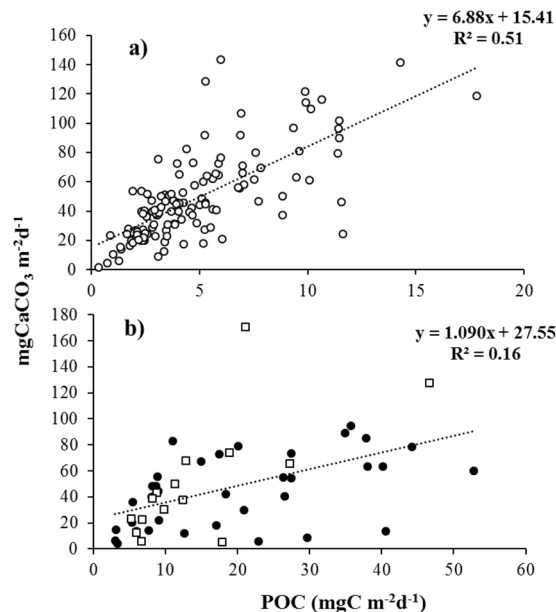


Figure 7. Linear correlations between total CaCO_3 and total POC fluxes obtained from sediment trap samples deployed at 2,300 m depth at the CQ site (a) and 1,000 (empty square) and 2,300 (black circles) m depths at the CC site (b) off Chile.

For the CQ site, fluxes of calcium carbonate and POC into sediment traps below 2,300 m were correlated ($y = 6.889x + 15.417$, $n = 127$; $R^2 = 0.51$) (Fig. 7a), which is consistent with published data for various geographic regions^{3,14,44–53}, like the PIC/POC ratios (Table 3). Some of these oceanic and coastal areas (such as the CQ site) exhibit relatively low productivity¹ that favours the export of CaCO_3 (mean $48.1 \text{ mg m}^{-2} \text{ d}^{-1}$) over POC (mean $4.7 \text{ mg m}^{-2} \text{ d}^{-1}$) (Fig. 5a,c) and possibly carbonate-driven POC export as the main ballast mechanism, which would explain the high PIC/POC ratio (>1) observed in this site. Thus, biominerals increase substantially sinking velocity because of their high densities and may serve to protect organic matter from degradation during transit to the ocean floor^{53–55}. Conversely, POC and CaCO_3 at CC, were not significantly correlated ($y = 1.090x + 27.56$, $n = 30$; $R^2 = 0.16$) (Fig. 7b), and the PIC/POC ratio was lower (<1) than the CQ site, which may be attributable to a very productive upwelling centre that supports massive diatom blooms¹ and favours the export of both CaCO_3 (mean $46.7 \text{ mg m}^{-2} \text{ d}^{-1}$) and POC (mean $19.7 \text{ mg m}^{-2} \text{ d}^{-1}$) (Fig. 6a,c) with perhaps silicate-driven POC export as the main ballast mechanism.

In the HCS, an average appendicularian abundance is estimated at 21.6 ind. m^{-3} ^{27,56} or $1,078 \text{ ind. m}^{-2}$ integrated down to 50 m depth (see www.st.nmfs.noaa.gov/copepod/atlas). On average, one appendicularian can produce between 7.3 and 10.1 FPa h^{-1} ^{27,57} or an average of 198.6 FPa d^{-1} or $72,500 \text{ FPa y}^{-1}$ (Supplementary Table S4). We estimated a total area of the HCS off Chile of $910,000 \text{ km}^2$, assuming a total latitudinal length of 2,600 km between 18.5° and 41.5°S and a width of 350 km ⁵⁸. Because most appendicularians occur within the upper 50 m of the water column^{59,60}, an estimate of 1.08×10^9 appendicularians within this upper layer would produce $7.12 \times 10^{19} \text{ FPa y}^{-1}$ along the whole HCS. Moreover, considering the size-spectrum of FPa found at both study sites (Fig. 2), we assumed that $\sim 90\%$ of the FPa produced are small FPa ($<100 \mu\text{m}$ of diameter) and 10% large. As the small FPa had an average biovolume and carbon content of 0.26 mg C mm^3 and 0.000364 mg C , respectively, while equivalent values for a large FPa were 0.041 mg C mm^3 and 0.0015 mg C (Fig. 3a and Supplementary Table 4). Finally, we estimated that $3.4 \times 10^{16} \text{ mg C y}^{-1}$ or 0.034 Gt C would be released annually as FPa in the upper 50 m water column of the HCS (Supplementary Table S4).

Given that the FPa vertical flux averaged $1.04 \text{ mg C m}^{-2} \text{ d}^{-1}$ (Figs 5b, 6b), we can estimate that $345.5 \times 10^6 \text{ kg}$ carbon (or 0.000345 Gt carbon) are exported annually down to 2,300 m depth in the HCS, which represents 1% of the FPa carbon standing stock within the upper 50 m of the water column, suggesting extensive recycling of FPa between the photic zone and deeper layers of the HCS (Supplementary Table 4). We lack data on POC fluxes and degradation rates between 2,300 m of depth and the sea floor (circa 4,500 m depth, in CQ and CC), but information on POC recycling in many disparate regions of the world oceans indicate that an additional POC loss of $\sim 30\%$ might occur⁶¹. This suggests that $\sim 0.7\%$ of the standing stock of the FPa-mediated carbon export from the upper 50 m stratum could reach the ocean floor along the HCS off Chile.

This is in line with reports suggesting that $<3\%$ of the generated upper production reaches bathypelagic depths ($>1,000 \text{ m}$) in the deep sea⁶², mainly due to the highly complex and variable food web in the water column⁶³ that removes most of the sinking particles, such as the FPa.

Our non-linear FPa-size derived carbon to volume ratio estimated an average POC flux in the HCS off Chile to be $345 \text{ kton C y}^{-1}$, twice as much the estimated with the linear model ($172 \text{ kton C y}^{-1}$). This study only includes the HCS off Chile, a very productive ecosystem that might differs from the rest of the global oceans (in food supply quality and quantity). Nevertheless, a widespread characteristic of the model is its non-linear, FPa-size derived nature, that we recommends to be considered for future estimated where FPa are key vehicles of PIC and/or POC carbon export.

Methods

Analysis of total POC and CaCO₃. Samples were obtained from sediment traps (SMT 230, Salzgitter Electronic, Kiel, equipped with 20 sample bottles) deployed at 2,300 m depth ~150 km off the CQ site (30°S, off Coquimbo city). At the CC site (36°, off Concepción city), the trap was initially deployed down to 1,000 m depth (2005–2006), but later moved down to 2,300 m depth (2006–2009). The water depths in the study sites were 4,700 m for CQ and 4,300 m for CC (Table 1). Sample collection cups were changed between 7 to 18 days in the CQ and 19 days for the CC site (Table 1). Before deployment, each collection cup was filled with a hypersaline NaCl–seawater solution (38–40 g kg⁻¹, prepared with water collected at 2000 m and 1% (v/v) saturated HgCl₂) to retard bacterial activity in the trap material⁶⁴. After recovery, the samples were poisoned again with HgCl₂ (0.5 mL/100 mL of seawater) and stored at 4 °C. In the laboratory, a fraction of the samples was split into aliquots by a rotary liquid splitter. The splitting procedure, sample preparation, and analysis were previously described⁶⁵. Subsequently, particulate organic carbon (POC) analyses were done after removal of CaCO₃ with HCL 2 N, while for total particulate carbon (TPC), part of the sample (e.g. 1/20 to 1/4,096) was filtered (pre-combusted GF/F Whatman) and dried at 50 °C. Later, these samples were analysed in a Carlo Erba C/N-analyser using acetanilide as a standard⁶. Finally, the TPC and POC data were converted by a stoichiometric balance for the final determination of the total particulate carbonate ((TPC-POC) x 8.3333)³.

Analysis of POC in FPa. Intact FPa (1,114 units, 528 from CQ and 586 from CC) of various sizes between 50 and 340 µm in diameter were isolated from sediment trap samples that covered most of the study period, and measured (major and minor axes of the FPa ellipsoid shape) by using a stereo microscope (Leica model MZ6). After a gentle wash with de-carbonated mineral water, using petri dish, to maintain the integrity of the FPa and photographed (Nikon Coolpix model 4500) using the stereo-microscope, then they were placed on 23 Whatman GF/F glass fibre filters in batches depending on their size (from 14 large to 142 small FPa). The images were processed in ImageJ software to estimate the volume of each faecal pellet and the total volume of each batch. Finally, subsamples of FPa on GF/F filters were acidified with 0.2 mL (~4 drops with a Pasteur pipette) of 2 N HCl to remove particulate inorganic carbon, washed with distilled water to remove excess acid, dried at 50 °C, and stored in hermetic plastic bottle with silica gel to await organic carbon (CHN) analysis, as described above. Due to the high variability in the diameters of the FPa used for elemental carbon analysis in the time series data from 1995 and 2004 (Fig. 2), average POCs of 0.26 mg mm⁻³ were used for small FPa (<100 µm diameter) and 0.041 mg mm⁻³ for large FPa (>100 µm diameter).

Total carbonate, coccolith abundance, and coccolithophore composition in FPa. 110 intact FPa (50–340 µm in diameter) were removed from sediment trap samples deployed at CQ (44 FPa pooled in 16 bunches) and CC (66 FPa pooled in 18 bunches) throughout the study period. This was made with the aid of a stereomicroscope (Leica model MZ6) at ×4 magnification and placed in a Petri dish with pre-filtered de-carbonated mineral water to prevent coccolith dissolution. Faecal pellets were washed five to eight times with filtered de-carbonated water and photographed. Images were processed with ImageJ software to estimate faecal pellet size and biovolume (Figs 2, 4) by applying prolate spheroid geometry⁶⁶.

In order to analyse the composition of coccospheres and coccoliths within FPa, 1–10 pellets (number depending on size) were removed from the Petri dish, gently placed in 2.5-mL vials containing 2 mL de-carbonated mineral water and sonicated at 50 to 60 Hz for 30 seconds⁶⁷. The contents of the vials were placed in sedimentation chambers and coccospheres and coccoliths identified and counted with an inverted microscope (×1,000 magnification). The coccoliths and coccospheres observed in a known area of the bottom of the chamber were counted and the data extrapolated to the total volume of the faecal pellets⁶. The samples also were examined by scanning electron microscopy to confirm the coccolithophore species identified with light microscopy. Finally, the number of coccoliths per coccolithophore species were transformed to CaCO₃ using conversion factors from the literature⁶⁸, and the result was extrapolated to the total biovolume of the FPa measured for each sample.

Statistical analyses. A Kolmogorov-Smirnov test (Minitab software) showed that our data for POC and CaCO₃ fluxes mediated by FPa in the CQ and CC sites were not distributed normally. We therefore used the non-parametric Mann Whitney test for multiple statistical comparisons (confidence limits set at 95%).

Received: 10 July 2018; Accepted: 12 October 2019;

Published online: 11 November 2019

References

1. Daneri, G. *et al.* Primary production and community respiration in the Humboldt Current System off Chile and associated oceanic areas. *Mar. Ecol. Prog. Ser.* **197**, 41–49 (2000).
2. Strub, P. T., Mesias, J. M., Montecino, V., Rutllant, J. & Salinas, S. The Sea (eds. Robinson, A. R., Brink, K. H.) 273–313 (John Wiley & Sons, Inc. 1998).
3. Hebbeln, D., Marchant, M. & Wefer, G. Seasonal variations of the particle flux in the Peru-Chile current at 30° S under “normal” and El Niño conditions. *Deep Sea Res. II* **47**, 2101–2128 (2000).
4. Silva, N., Rojas, N. & Fedele, A. Water masses in the Humboldt Current System: Properties, distribution, and the nitrate deficit as a chemical water mass tracer for Equatorial Subsurface Water off Chile. *Deep-Sea Res.* **56**, 1004–1020 (2009).
5. Hormazabal, S., Shaffer, G. & Leth, O. Coastal transition zone off Chile. *J. Geophys. Res.* **109**, 1–13 (2004).
6. Menschel, E., González, H. E. & Giesecke, R. Coastal-ocean distribution of coccolithophores and their role in the carbonate flux ratio of the Concepción, Chile, upwelling area (36°S). *J. Plankton Res.* **38**(4), 798–817 (2016).
7. Walsh, I. D. & Gardner, W. D. A comparison of aggregate profiles with sediment trap fluxes. *Deep-Sea Res.* **39**, 1817–1834 (1992).
8. Lutz, M., Dunbar, R. & Caldeira, K. Regional variability in the vertical flux of particulate organic carbon in the ocean interior. *Global Biogeochem. Cycles* **16**, 11–15 (2002).
9. Muller-Karger, F. E. *et al.* The importance of continental margins in the global carbon cycle. *Geophys. Res. Lett.* **32**, 1–4 (2005).

10. Grönwald, A., Morales, C., González, H. E., Sylvester, C. & Castro, L. Grazing impact of copepod assemblages and gravitational flux in coastal and oceanic waters off central Chile during two contrasting seasons. *J. Plankton Res.* **24**, 55–68 (2002).
11. González, H. E., Menschel, E., Aparicio, C. & Barriá, C. Spatial and temporal variability of microplankton and detritus, and their export to the shelf sediments in the upwelling area off Concepción, Chile (36°S), during 2002–2005. *Prog. Oceanogr.* **75**, 435–451 (2007).
12. González, H. E. *et al.* Carbon fluxes within the epipelagic zone of the Humboldt Current System off Chile: The significance of euphausiids and diatoms as key functional groups for the biological pump. *Prog. Oceanogr.* **83**, 217–227 (2009).
13. Turner, J. T. Zooplankton fecal pellets, marine snow, phytodetritus and the ocean's biological pump. *Prog. Oceanogr.* **130**, 205–248 (2015).
14. González, H. E., Hebbeln, D., Iriarte, J. L. & Marchant, M. Downward fluxes of faecal material and microplankton at 2,300 m depth in the oceanic area off Coquimbo (30°S), Chile, during 1993–1995. *Deep-Sea Res. II* **51**, 2457–2474 (2004).
15. González, E., Ortíz, V. C. & Sobarzo, M. The role of faecal material in the particulate organic carbon flux in the northern Humboldt Current, Chile (23°S), before and during the 1997–1998 El Niño. *J. Plankton Res.* **22**, 499–529 (2000).
16. Boyd, P. W. & Newton, P. P. Does planktonic community structure determine downward particulate organic carbon flux in different oceanic provinces. *Deep-Sea Res. Part I* **46**, 63–91 (1999).
17. González, H. E. *et al.* Producción primaria y su destino en la trama trófica pelágica y océano profundo e intercambio océano-atmósfera de CO₂ en la zona norte de la Corriente de Humboldt (23°S): posibles efectos del evento El Niño, 1997–98 en Chile. *Rev. Chil. Hist. Nat.* **71**, 429–458 (1998).
18. Escribano, R. *et al.* Biological and chemical consequences of the 1997–1998 El Niño in the Chilean coastal upwelling system: a synthesis. *Deep-Sea Res. II* **51**, 2389–2411 (2004).
19. Bidigare, R. R. & Ondrusel, M. E. Spatial and temporal variability of phytoplankton pigment distribution in the central equatorial Pacific Ocean. *Deep-Sea Res.* **43**, 809–833 (1996).
20. Carr, M.-E. Simulation of carbon pathways in the planktonic ecosystem off Peru during the 1997–1998 El Niño and La Niña. *J. Geophys. Res.* **108**(C12), 3380 (2003).
21. González, H. The distribution and abundance of krill faecal material and oval pellets in the Scotia and Weddell Seas (Antarctica) and their role in particle flux. *Polar Biol.* **12**, 81–91 (1992a).
22. Turner, J. T. & Ferrante, J. G. Zooplankton fecal pellets in aquatic ecosystems. *BioScience*. **29**, 670–677 (1979).
23. Turner, J. T. Zooplankton fecal pellet, marine snow and sinking phytoplankton blooms. *Aquat. Microb. Ecol.* **27**, 57–102 (2002).
24. Steele, J. H. & Baird, I. E. Sedimentation of organic matter in a Scottish sea loch. *Mem. Ist. Ital. Idrobiol.* **29**(Suppl), 73–88 (1972).
25. Lane, P. V. Z., Smith, S. L., Urban, J. L. & Biscayn, P. E. Carbon flux and recycling associated with zooplanktonic fecal pellets on the shelf of the Middle Atlantic Bight. *Deep-Sea Res. II* **41**, 437–457 (1994).
26. González, H. E. Distribution and abundance of minipellets around the Antarctic Peninsula. Implications for protistan feeding behavior. *Mar. Ecol. Prog. Ser.* **90**, 223–236 (1992).
27. Vargas, C. A. *et al.* Importance of copepods versus appendicularians in vertical carbon fluxes in a Swedish fjord. *Mar. Ecol. Prog. Ser.* **241**, 125–138 (2002).
28. Berline, L., Stemmann, L., Vichi, M., Lombard, F. & Gorsky, G. Impact of appendicularians on detritus and export fluxes: a model approach at DyFAMed site. *J. Plankton Res.* **33**, 855–872 (2011).
29. Honjo, S. Coccoliths: production, transportation and sedimentation. *Mar. Micropaleontol.* **1**, 65–77 (1976).
30. Baumann, K.-H., Andruleit, H., Böckel, B., Geisen, M. & Kinkel, H. The significance of extant coccolithophores as indicators of ocean water masses, surface water temperature, and paleoproductivity: a review. *Paläontol. Zeitschrift*. **79**(1), 93–112 (2005).
31. de Vargas, C., Aubry, M.-P., Probert, I. & Young, J. Evolution of Primary Producers in the Sea (eds. Falkowski, P. G. & Knoll, A. H.) 251–285 (Elsevier, New York, 2007).
32. González, H. E. & Smetacek, V. The possible role of the cyclopoid copepod *Oithona* in retarding vertical flux of zooplankton faecal material. *Mar. Ecol. Prog. Ser.* **113**, 233–246 (1994).
33. Klaas, C. & Archer, D. E. Association of sinking organic matter with various types of mineral ballast in the deep sea: Implications for the rain ratio. *Global Biogeochem. Cycles* **16**, 1116 (2002).
34. Poulsen, L. K. & Kiorboe, T. Vertical flux and degradation rate of copepod fecal pellets in a zooplankton community by small copepods. *Mar. Ecol. Prog. Ser.* **323**, 195–204 (2006).
35. Svendsen, C., Wexels, C., Reigstad, M. & Seuthe, L. Degradation of copepod faecal pellets in the upper layer: role of microbial community and *Calanus finmarchicus*. *Mar. Ecol. Prog. Ser.* **462**, 39–49 (2012).
36. Bach, L. T. *et al.* An approach for particle sinking velocity measurements in the 3–400 µm size range and considerations on the effect of temperature on sinking rates. *Mar. Biol.* **159**, 1853–1864 (2012).
37. Deibel, C. & Powell, L. Ultrastructure of the pharyngeal filter of the appendicularian *Oikopleura vanhoeffeni*: Implications for particle size selection and fluid mechanics. *Mar. Ecol. Prog. Ser.* **35**, 243–250 (1987).
38. Durkin, C. A., Van Mooy, B. A. S., Dyhrman, S. T. & Buesseler, K. O. Sinking phytoplankton associated with carbon flux in the Atlantic Ocean. *Limnol. Oceanogr.* **61**, 1172–1187 (2016).
39. Trull, T. W. *et al.* *In situ* measurement of mesopelagic particle sinking rates and the control of carbon transfer to the ocean interior during the Vertical Flux in the Global Ocean (VERTIGO) voyages in the North Pacific. *Deep-Sea Res. Part II* **55**, 1684–1695 (2008).
40. Castilla, J. C. & Camus, P. A. The Humboldt El Niño scenario: Coastal benthic resources and anthropogenic influences, with particular reference to the 1982/83 ENSO. *S. Afr. J. Sci.* **12**, 703–712 (1992).
41. Espinoza-Morrigerón, D. *et al.* Impacts of El Niño events on the Peruvian upwelling systems productivity. *J. Geophys. Res.* **122**, 5423–5444 (2017).
42. Fernandez, D., Lopez-Urrutia, A., Fernandez, A., Acuña, J. L. & Harris, R. Retention efficiency of 0.2 to 0.6 µm particles by the appendicularians *Oikopleura dioica* and *Fritillaria borealis*. *Mar. Ecol. Prog. Ser.* **266**, 89–101 (2004).
43. Ulloa, O. *et al.* Evolution and biological effects of the 1997–98 El Niño in the upwelling ecosystem off northern Chile. *Geophys. Res. Lett.* **28**, 1591–1594 (2001).
44. Ploug, H., Iversen, M. H. & Fischer, G. Ballast, sinking velocity, and apparent diffusivity within marine snow and zooplankton fecal pellets: Implications for substrate turnover by attached bacteria. *Limnol. Oceanogr.* **53**, 1878–1886 (2008).
45. Honjo, S. Seasonality and interaction of biogenic and lithogenic particulate flux at the Panama Basin. *Science* **218**, 883–884 (1982).
46. Honjo, S. Global Ocean Flux Study. Proceeding of a Workshop Natural Academic. 305–324 (National Academy Press, Washington D.C., 1984).
47. Nair, R. R. *et al.* Increased particle flux to the deep ocean related to monsoons. *Nature* **338**, 749–751 (1989).
48. Honjo, S., Dymond, J., Collier, R. & Manganini, S. J. Export production of particles to the interior of Equatorial Pacific Ocean during 1992 EqPac Experiment. *Deep-Sea Res. II* **42**, 831–870 (1995).
49. Ittekkot, V. *et al.* Enhanced particle fluxes in Bay of Bengal induced by injection of water. *Nature* **351**, 385–387 (1991).
50. Honjo, S., Francois, R., Manganini, S., Dymond, J. & Collier, R. Export fluxes in the Western Pacific Sector of the Southern Ocean along 170°W. *Deep Sea Res. II* **47**, 3521–3548 (2000).
51. Conte, M. H., Ralph, N. & Ross, E. H. Seasonal and interannual variability in deep ocean particle fluxes at the Oceanic Flux Program (OFP)/Bermuda Atlantic Time Series (BATS) site in the western Sargasso Sea near Bermuda. *Deep-Sea Res. II* **48**, 1471–1505 (2001).
52. Hung, J.-J., Lin, C.-S., Chung, Y.-C., Hung, G.-W. & Liu, W.-S. Lateral fluxes of biogenic particles through the Mien-Hua canyon in the southern East China Sea slope. *Cont. Shelf Res.* **23**, 935–955 (2003).
53. Ramaswamy, V. & Gaye, B. Regional variations in the fluxes of foraminifera carbonate, coccolithophorid carbonate and biogenic opal in the northern Indian Ocean. *Deep-Sea Res. I* **53**, 271–293 (2006).

54. Armstrong, R. A., Lee, C., Hedges, J. I., Honjo, S. & Wakeham, S. G. A new, mechanistic model for organic matter carbon fluxes in the ocean based on the quantitative association of POC with ballast minerals. *Deep-Sea Res. II*. **49**, 219–236 (2002).
55. Bathmann, U. V., Noji, T. T., Voss, M. & Peinert, R. Copepod fecal pellets: abundance, sedimentation and content at a permanent station in the Norwegian Sea in May/June 1986. *Mar. Ecol. Prog. Ser.* **38**, 45–51 (1987).
56. Aravena, G. & Palma, S. Taxonomic identification of appendicularians collected in the epipelagic waters off northern Chile (Tunicata, Appendicularia). *Rev. Chil. Hist. Nat.* **75**, 307–325 (2002).
57. Taguchi, S. Seasonal study of fecal pellets and discarded houses of Appendicularia in a subtropical inlet, Kaneohe Bay, Hawaii. *Est. coastal Shelf Sci.* **14**, 545–555 (1982).
58. Fuenzalida, R., Schneider, W., Garcés-Vargas, J. & Bravo, L. Satellite altimetry data reveal jet-like dynamics of the Humboldt Current. *J. Geophys. Res.* **113**, C07043 (2008).
59. Fenaux, R. Quelques aspects de la distribution verticale chez les appendiculaires en Méditerranée. *Cah. Biol. Mar.* **9**, 23–29 (1968).
60. Tomita, M., Shiga, N. & Ikeda, T. Seasonal occurrence and vertical distribution of appendicularians in Toyama Bay, southern Japan Sea. *J. Plankton Res.* **25**, 579–589 (2003).
61. Wakeham S. G. & Lee C. *Organic Geochemistry* (eds Engel M. H., Macko S. A.) 145–165 (Springer, Boston, 1993).
62. De La Rocha, C. & Passow, U. Factors influencing the sinking of POC and the efficiency of the biological carbon pump. *Deep-Sea Res. II*. **54**, 639–658 (2007).
63. Legendre, L. & Rivkin, R. B. Fluxes of carbon in the upper ocean: regulation by food-web control nodes. *Mar. Ecol. Prog. Ser.* **242**, 95–109 (2002).
64. Lee, C., Hedges, J. I., Wakeham, S. G. & Zhu, N. Effectiveness of various treatments in retarding microbial activity in sediment trap material and their effects on the collection of swimmers. *Limnol. Oceanogr.* **37**, 117–130 (1992).
65. Wefer, G. & Fischer, G. Annual primary production and export flux in the Southern Ocean from sediment trap data. *Mar. Chem.* **35**, 597–613 (1991).
66. Sun, J. & Lui, D. Geometric models for calculating cell biovolume and surface area for phytoplankton. *J. Plankton Res.* **25**, 1331–1346 (2003).
67. Bairbakhish, A. N., Bollmann, J., Sprengel, C. & Thierstein, H. R. Disintegration of aggregates and coccospores in sediment trap samples. *Mar. Micropaleontol.* **37**, 219–223 (1999).
68. Young, J. R. & Ziveri, P. Calculation of coccolith volume and its use in calibration of carbonate flux estimates. *Deep-Sea Res. II*. **47**, 1679–1700 (2000).

Acknowledgements

We thank the captain and crew of the R/V AGOR Vidal Gormáz for their help during sampling. We are grateful to Mr. Ricardo Silva, who assisted us with sample preparation and observations during the scanning electron microscope analysis at UACH, and Dr. O. Pizarro, M. Marchant, D. Hebbeln and C. Hormazábal, who helped during the deployment and retrieval of the deep sediment trap. The POC and carbonate data for the CQ site were measured at the AWI- Bremerhaven, where our former collaborators, Drs. D. Hebbeln and M. Marchant, deserve our deep gratitude. Special thanks are due to Dr. Lluïsa Cros (ICM, Barcelona, Spain) for her valuable collaboration in methodology for studying coccolithophores and in their identification. Editorial services were provided by Sea Pen Scientific Writing and the English grammar was polished by Dr. R. Thompson. Several projects contributed with funds (partial financial support) at different stages of the time series: FONDAP-COPAS (150100007), FIP (2004-20), Ocean Certain (EU-FP7 N°603773), COPAS-Sur Austral Basal (PFB-31); FONDAP-IDEAL (15150003). EM acknowledges a fellowship provided by CONICYT to conduct graduate studies at the Universidad de Concepción.

Author contributions

H.E.G. was responsible for acquiring funding and for sampling methods and design; E.M. collected the samples and analysed the data; H.E.G. and E.M. designed the moorings and co-wrote the paper.

Competing interests

The authors declare no competing interests.

Additional information

Supplementary information is available for this paper at <https://doi.org/10.1038/s41598-019-52469-y>.

Correspondence and requests for materials should be addressed to H.E.G.

Reprints and permissions information is available at www.nature.com/reprints.

Publisher's note Springer Nature remains neutral with regard to jurisdictional claims in published maps and institutional affiliations.



Open Access This article is licensed under a Creative Commons Attribution 4.0 International License, which permits use, sharing, adaptation, distribution and reproduction in any medium or format, as long as you give appropriate credit to the original author(s) and the source, provide a link to the Creative Commons license, and indicate if changes were made. The images or other third party material in this article are included in the article's Creative Commons license, unless indicated otherwise in a credit line to the material. If material is not included in the article's Creative Commons license and your intended use is not permitted by statutory regulation or exceeds the permitted use, you will need to obtain permission directly from the copyright holder. To view a copy of this license, visit <http://creativecommons.org/licenses/by/4.0/>.

© The Author(s) 2019